SHILTON, M. G. & HOWE, A. T. (1977). *Mater. Res. Bull.* **12**, 701-706.
THÉRY, J. & BRIANÇON, D. (1962). *C. R. Acad. Sci.* **254**, 2782-2784.
THOMAS, J. O. & FARRINGTON, G. C. (1983). *Acta Cryst.* B**39**, 227-235.
YAO, Y. Y. & KUMMER, J. T. (1967). *J. Inorg. Nucl. Chem.* **29**, 2453-2475.

Acta Cryst. (1986). B**42**, 229-236

An Analysis of the Structural Characteristics of Hollandite Compounds

BY ROBERT W. CHEARY

School of Physics and Materials, New South Wales Institute of Technology, PO Box 123, *Broadway, New South Wales, Australia* 2007

(*Received* 29 *April* 1985; *accepted* 18 *November* 1985)

Abstract

Neutron powder diffraction data for seven SYNROC-related barium hollandites $Ba_x(M^{3+}Ti^{4+})_8O_{16}$ have been refined to establish how various trivalent ions such as Fe, Al and Ga change the crystal structure and predispose it to radwaste substitution. Particular attention is given to changes in the environment of the tunnel sites and the nature of the monoclinic-tetragonal transformation in hollandites. Structural data from earlier refinements are included in the analysis. The unit-cell volume, the lattice parameter of the unique axis, the O octahedral volume and the tunnel-cavity volume are all controlled primarily by the size of the octahedral-site cations. The change from tetragonal to monoclinic symmetry occurs when the tunnel cations are no longer able to support the tunnel walls which collapse onto the tunnel ions with the corner linkages between the walls acting as hinges.

Introduction

The synthetic mineral assemblage known as SYNROC is currently being evaluated for the immobilization of radioactive wastes (*e.g.* Kesson & Ringwood, 1984). In this material barium hollandite is used as the host for large cations such as Cs and Rb. The unit-cell formula of hollandites is $A_xB_8O_{16}$ ($x \leq 2$) where A represents ions in the tunnel cavities of the structure (*e.g.* Ba, Cs) and B are smaller cations occupying octahedral sites such as Al^{3+}, Ti^{3+} and Ti^{4+} (Kesson, 1983). They may be tetragonal [$I4/m$, a = 9·90 to 10·10 Å and c = 2·9 to 3·0 Å (Byström & Byström, 1950; Dryden & Wadsley, 1958; Sinclair, McLaughlin & Ringwood, 1980)] or monoclinic [$I2/m$, β = 90 to 91·5° (Cadée & Verschoor, 1978; Post, Von Dreele & Buseck, 1982)]. The symmetry is usually monoclinic when the ratio of the cation radii $R_A/R_B < 2{\cdot}08$ and tetragonal when this ratio $> 2{\cdot}08$ although this is by no means a general rule for all hollandites (Post *et al.*, 1982). In their analysis of radwaste substitution in SYNROC, Kesson (1983) and Kesson & White (1986) have shown that high concentrations of Cs can be immobilized in host hollandites containing Ti^{3+} on the B sites. The majority of hollandites considered in this context are in the solid-solution range between tetragonal $Ba_x(Al^{3+}Ti^{4+})_8O_{16}(x = 1{\cdot}14)$ and monoclinic $Ba(Ti^{3+}Ti^{4+})_8O_{16}$. Presumably, the effect of large ions such as Ti^{3+} on the B sites is to increase the unit-cell volume and enlarge the A-site tunnel cavities thereby facilitating the inclusion of Cs into the structure.

The objective of the present work is to examine how the barium hollandite structure responds to various combinations of M^{3+} and Ti^{4+} ions on the B sites. Particular attention is focused on the following aspects of the structure: the way in which the size and shape of the tunnel sites and the surrounding O octahedral framework change, the factors controlling the monoclinic-tetragonal transformation, and the changes that occur during a structural transformation. Altogether seven barium hollandite structures have been refined, four monoclinic and three tetragonal, from high-resolution neutron powder diffraction data with M = Ga, Al, Fe and varying proportions of Fe and Al. Results from earlier refinements have also been included in this analysis.

Sample preparation and measurement conditions

Initially four barium hollandite specimens were prepared, three tetragonal with M = Al, at two values of x, and Ga (Guha, Kolar & Volavsek, 1976; Cheary, Hunt & Calaizis, 1981; Roth, 1981; Bursill & Grzinic, 1980), and one monoclinic with M = Fe (Cadée & Verschoor, 1978). Three of them were prepared by mixing the starting materials $BaCO_3$, TiO_2 and the appropriate sesquioxide (Al_2O_3, Fe_2O_3 or Ga_2O_3) to give hollandites with x = 1·33 Ba ions per unit cell, *viz.*

$$BaCO_3 + M_2O_3 + 4TiO_2.$$

0108-7681/86/030229-08$01.50

The fourth hollandite was prepared with M = Al, but with $x = 1{\cdot}14$ Ba ions per unit cell, *viz.*

$$BaCO_3 + M_2O_3 + 5TiO_2.$$

The starting mixtures were homogenized by wet grinding with acetone in a tungsten carbide ball mill and then calcined at 1073 K for 4 h. After further wet grinding the specimens were fired in air at 1593 K for 12 h. X-ray diffraction scans of the final products revealed well crystallized and substantially single-phase hollandites of the expected symmetry. The patterns of the specimens with $x = 1{\cdot}33$ contained weak additional diffraction lines from a second phase, possibly the spinel phase BaM_2O_4, but it was not possible to make a positive identification of this phase owing to the scarcity and low intensity of the lines. In these three specimens the actual x was therefore expected to be less than the nominal value 1·33. This was confirmed by the refinement of the neutron diffraction data (see Table 2) which indicated x values of 1·23, 1·26 and 1·28 for the barium aluminium, barium gallium and barium iron hollandites, respectively. When these compounds are prepared at the concentration levels obtained from refinement no second-phase diffraction lines are observed. Refinement of the neutron data from the other barium aluminium hollandite (nominally $x = 1{\cdot}14$) indicated an actual cell composition with $x = 1{\cdot}12$.

Specimens were also prepared in the solid-solution range between tetragonal $Ba_{1{\cdot}23}(AlTi)_8O_{16}$ and monoclinic $Ba_{1{\cdot}28}(FeTi)_8O_{16}$ to examine the tetragonal–monoclinic transformation, *viz.*

$$[Ba_{1{\cdot}28}(FeTi)_8O_{16}]_Q + [Ba_{1{\cdot}23}(AlTi)_8O_{16}]_{1-Q}$$

with $Q = 0{\cdot}115$, 0·232, 0·352, 0·473, 0·602, 0·730 and 0·860. As a group these specimens will be referred to as $Ba([AlFe]_QTi)_8O_{16}$. X-ray diffraction scans of these specimens revealed single-phase tetragonal hollandites for $Q \leq 0{\cdot}473$ and single-phase monoclinic hollandites for $Q \geq 0{\cdot}602$.

Neutron diffraction data were collected for seven of the eleven specimens using the multidetector high-resolution powder diffractometer at Lucas Heights (Howard, Ball, Davis & Elcombe, 1983) at an incident wavelength of 1·500 Å. All the measurements were carried out at room temperature (296–298 K) with finely ground specimens compacted in a thin-walled vanadium can mounted on the rotating stage of the diffractometer. Data were recorded for fixed monitor counts at 0·05° 2θ intervals over the angular range $2\theta = 0$ to 150°. The rest of the specimens [*i.e.* $Ba([AlFe]_QTi)_8O_{16}$ with $Q = 0{\cdot}115$ to 0·473, inclusive] were examined by X-ray powder diffraction to determine lattice parameters only. It should be noted that the abbreviated hollandite formula given above [*viz.* $Ba_x(M^{3+}Ti^{4+})_8O_{16}$] is used throughout this paper and actually corresponds to $Ba_x(M_{2x}Ti_{8-2x})O_{16}$.

Refinement procedure

All the neutron diffraction data were refined by the Rietveld method (Rietveld, 1969) using the program developed by Wiles & Young (1981) and implemented at the Australian Atomic Energy Commission by Drs R. J. Hill and C. J. Howard. In the present analysis the diffraction profiles were fitted by a sum of Gaussians (Howard, 1982) whilst the background counts were fitted with a polynomial in 2θ. The goodness-of-fit indicators quoted later are the weighted pattern R factor R_{wp}, the expected value R_{wp}^E based on the neutron count statistics, and the Bragg R factor R_B.

Good fits were obtained for all the diffraction patterns with R_{wp} values between 6 and 8% with corresponding expected values between 5 and 7%. The Bragg R factor was typically below 2·8%. In the three specimens containing a small amount of second-phase material, those regions containing impurity lines were excluded from the refinement. To facilitate comparison between the tetragonal and monoclinic hollandites, refinement was carried out using the coordinate scheme for $I2/m$ given in Cadée & Verschoor (1978) with constraints between related atomic coordinates and lattice parameters being incorporated in the refinement of the tetragonal hollandites to reflect their $I4/m$ symmetry. Constraints were also placed on the occupancy levels of the A and B sites to maintain charge neutrality over the unit cell and a total of eight ions on the B sites. The Ba ions and B ions were assumed to be randomly distributed over their respective sites. Although refinement of the anisotropic temperature factors was possible, it was normally halted once stable isotropic temperature factors were obtained. In general the precision of the anisotropic temperature factors was poor (typically >20%) and no significant improvement in the fit followed from their inclusion. Lattice parameters were determined as part of the refinement program. In the case of the four hollandites for which neutron data were not available the lattice parameters were measured using a least-squares fitting procedure to the Cu $K\alpha_1$ peak positions of the stronger X-ray diffraction lines below $2\theta = 120°$ with corrections being made for instrumental aberrations (Klug & Alexander, 1974).

The coordinates of the B ions in $Ba_x(GaTi)_8O_{16}$ and $Ba([AlFe]_QTi)_8O_{16}$ with $Q = 0{\cdot}602$, 0·730 and 0·860 could not be refined to physically sensible values as the negative scattering length of the Ti cancels the positive scattering length of the other ions on this site giving a resultant scattering length close to zero. The B-site coordinates quoted in Table 2 for barium gallium hollandite represent nominal values for a tetragonal hollandite. The standard errors quoted reflect the spread of these coordinates over all the previous refinements which have all been in

Table 1. *Observed cell constants and unit-cell volumes of barium hollandites*

The type of cell is indicated by a *T* for tetragonal and *M* for monoclinic. Under the heading of method, *N* refers to values given by Rietveld refinement of neutron data ($\lambda = 1{\cdot}500$ Å) whereas *X* refers to values given by least-squares fitting of peak positions of X-ray powder data ($\lambda = 1{\cdot}54056$ Å).

Specimen	Type	Method	a(Å)	b(Å)	c(Å)	β(°)	V(Å^3)
$Ba_{1\cdot26}(GaTi)_8O_{16}$	*T*	*N*	10·0450 (4)	2·9640 (1)			299·07 (3)
$Ba_{1\cdot12}(AlTi)_8O_{16}$	*T*	*N*	9·9750 (2)	2·92541 (5)			291·08 (2)
$Ba[(AlFe)_QTi]_8O_{16}$							
Q							
0	*T*	*N*	9·9485 (2)	2·9242 (1)			289·42 (2)
0·115	*T*	*X*	9·9640 (3)	2·9266 (11)			290·56 (12)
0·232	*T*	*X*	9·9855 (5)	2·9351 (17)			292·66 (18)
0·352	*T*	*X*	10·0020 (5)	2·9415 (20)			294.27 (23)
0·473	*T*	*X*	10·0174 (6)	2·9466 (25)			295·69 (28)
0·602	*M*	*N*	10·0469 (6)	2·9561 (2)	10·0308 (7)	90·043 (4)	297·91 (6)
0·730	*M*	*N*	10·1169 (11)	2·9630 (3)	9·9931 (10)	90·396 (3)	299·55 (9)
0·860	*M*	*N*	10·1799 (8)	2·9695 (2)	9·9583 (7)	90·707 (3)	301·01 (7)
1	*M*	*N*	10·2378 (5)	2·9783 (2)	9·9200 (5)	91·019 (2)	302·43 (5)

Table 2. *Structural parameters for barium hollandites obtained by Rietveld refinement of neutron diffraction data* ($\lambda = 1{\cdot}5000$ Å)

All atomic coordinates are expressed in terms of a unit cell with *I*2/*m* symmetry. B_{iso} refers to the isotropic temperature factors in Å^2.

			$Ba(AlFeTi)_QO_{16}$				
	$Ba(GaTi)O_{16}$	$Ba[Al(2)Ti]O_{16}$	$Q = 0$	$Q = 0{\cdot}602$	$Q = 0{\cdot}730$	$Q = 0{\cdot}860$	$Q = 1$
Ba	1·259 (11)	1·121 (18)	1·227 (20)	1·234 (10)	1·239 (10)	1·246 (10)	1·282 (10)
Ga	2·518 (22)	—	—	—	—	—	—
Al	—	2·242 (36)	2·454 (40)	0·940 (20)	0·631 (20)	0·325 (20)	—
Fe	—	—	—	1·527 (20)	1·847 (20)	2·166 (20)	2·565 (20)
Ti	5·482	5·758	5·546 (40)	5·533 (20)	5·522 (20)	5·509 (20)	5·435 (20)
A site							
y	0·134 (7)	0·094 (4)	0·141 (3)	0·125 (8)	0·145 (7)	0·136 (5)	0·131 (5)
B_{iso}	3·0 (7)	1·8 (4)	1·9 (4)	3·4 (1.1)	2·8 (9)	3·2 (9)	1·4 (5)
*B*1 site							
x	0·330 (10)	0·3308 (6)	0·3340 (9)	0·3360 (15)	0·3370 (15)	0·3380 (15)	0·3390 (20)
z	0·1480 (10)	0·1454 (7)	0·1477 (10)	0·1468 (15)	0·1465 (15)	0·1462 (15)	0·1460 (15)
B_{iso}	—	1·22 (13)	1·27 (14)	—	—	—	0·85 (10)
*B*2 site							
x	0·8520 (10)	0·8546 (7)	0·8523 (10)	0·8532 (20)	0·8535 (20)	0·8538 (25)	0·8540 (25)
z	0·3330 (10)	0·3308 (6)	0·3340 (9)	0·3355 (15)	0·3365 (18)	0·3375 (20)	0·3383 (20)
B_{iso}	—	1·22 (13)	1·27 (14)	—	—	—	0·85 (10)
O1 site							
x	0·2986 (4)	0·2982 (1)	0·2989 (3)	0·2983 (9)	0·2984 (5)	0·2964 (5)	0·2951 (5)
z	0·3471 (5)	0·3456 (2)	0·3455 (3)	0·3481 (8)	0·3491 (5)	0·3497 (4)	0·3499 (4)
B_{iso}	0·48 (5)	0·52 (4)	0·48 (3)	0·99 (16)	0·82 (9)	0·73 (8)	0·97 (8)
O2 site							
x	0·0402 (4)	0·0414 (1)	0·0412 (2)	0·0416 (8)	0·0409 (4)	0·0409 (5)	0·0410 (4)
z	0·3323 (5)	0·3344 (2)	0·3347 (3)	0·3312 (8)	0·3283 (5)	0·3255 (4)	0·3205 (4)
B_{iso}	0·91 (8)	0·59 (6)	0·59 (4)	0·85 (16)	0·52 (9)	0·83 (9)	0·35 (7)
O3 site							
x	0·6677 (5)	0·6656 (2)	0·6653 (3)	0·6622 (9)	0·6620 (5)	0·6599 (4)	0·6550 (4)
z	0·0402 (4)	0·0414 (1)	0·0412 (2)	0·0412 (7)	0·0405 (4)	0·0407 (4)	0·0404 (4)
B_{iso}	0·91 (8)	0·59 (6)	0·59 (4)	0·70 (15)	0·59 (9)	0·85 (9)	0·67 (7)
O4 site							
x	0·6529 (5)	0·6544	0·6545 (3)	0·6550 (10)	0·6558 (6)	0·6575 (5)	0·6592 (5)
z	0·2986 (4)	0·2982	0·2989 (3)	0·3006 (9)	0·3008 (4)	0·3024 (4)	0·3025 (4)
B_{iso}	0·48 (5)	0·52 (4)	0·48 (3)	1·31 (17)	1·03 (10)	0·86 (9)	0·93 (7)
Goodness of fit(%)							
R_{WP}	8·40	5·90	7·90	7·13	7·67	7·04	6·67
R^E_{WP}	5·36	4·61	4·91	5·91	6·46	5·77	5·25
R_B	2·38	2·10	1·67	2·26	2·32	2·50	2·76

the range $x = 0{\cdot}3308$ to $0{\cdot}3340$ and $z = 0{\cdot}1455$ to $0{\cdot}1488$ (Byström & Byström, 1950; Dryden & Wadsley, 1958; Sinclair *et al.*, 1980; Sabine & Hewat, 1982; Post *et al.*, 1982; Cheary & Kwiatkowska, 1984). The *B*-site coordinates of the monoclinic hollandites $Ba([AlFe]_QTi)_8O_{16}$, with $Q < 1$, were obtained by interpolating between the coordinates of the end members (*i.e.* $Q = 0$ and 1). The shape of the interpolation function for each *B* coordinate was matched to the variation of an associated O possessing similar changes over this range. The standard errors quoted represent the combined errors of the end-member coordinates reflected through the interpolation calculation.

All the results obtained from the Rietveld refinement of the seven barium hollandites are collected together in Tables 1 and 2 along with the lattice parameters calculated from X-ray data.

The hollandite structure: terminology

In the $I2/m$ representation of the hollandite structure the tunnels form along the b axis. Within the hollandite tunnels the A ions are held within box-shaped cavities of eight O ions and tend to occupy one of two equally probable off-centre positions (*i.e.* $0, \pm y, 0$). Each tunnel is defined by four walls, referred to here as the octahedral walls, linked together by corner-shared O octahedra [this is well illustrated in Fig. 1 of Kesson (1983)]. Within each octahedral wall there are two columns of O octahedra connected together by edge sharing but displaced by $b/2$ with respect to each other. All the O octahedra within a single wall are identical, but distorted owing to the contraction of the common edge between the columns. In tetragonal hollandites all the O octahedra in a unit cell are identical. In monoclinic hollandites only those on opposite walls are identical and as such the structure consists of two different types of octahedra which are referred to as S-type and T-type octahedra. These are shown in the (010) projection of the hollandite structure, Fig. 1, which also identifies similar O–O interatomic distances and defines the various O positions, B sites and bond angles referred to below.

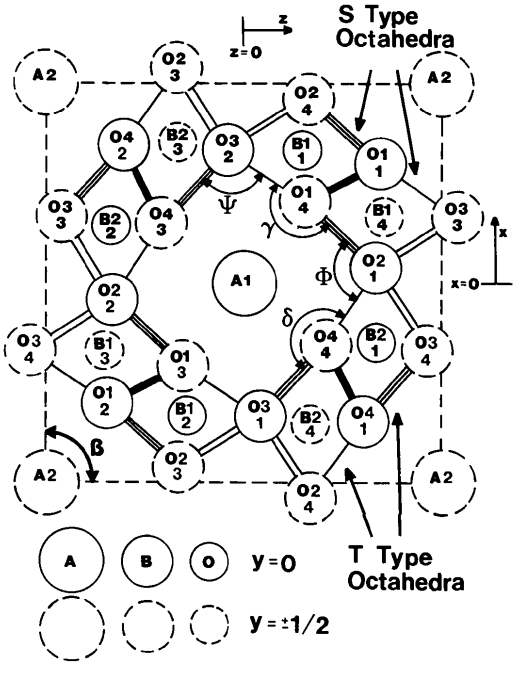

Fig. 1. Projection of the hollandite structure onto the (010) plane showing the various atomic positions, bond angles and O octahedra referred to throughout the paper. O–O bonds depicted with similar line patterns have the same bond length in tetragonal hollandites. In monoclinic hollandites the S- and T-type octahedra are different.

Discussion of the influence of the B–O bond length on the structure

The average size of the B cations is of central importance to many of the properties of the hollandite structure. This is illustrated in Figs. 2 and 3 where the unit-cell volume V_c, the lattice parameter b, the O octahedral volume V_O per unit cell and the A-site cavity volume V_A are plotted against the average B–O bond length. The term octahedral volume per unit cell used here refers to the volume contained within

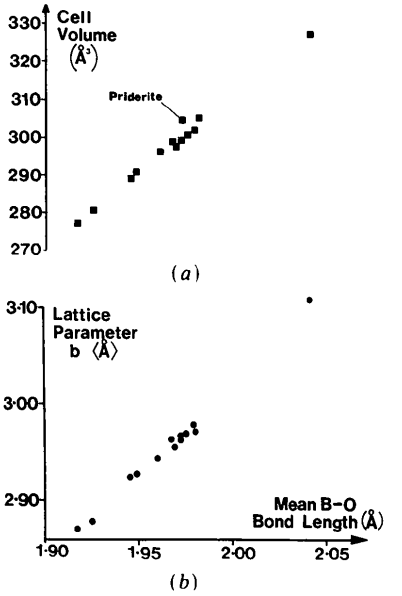

Fig. 2. (*a*) Unit-cell volume V_c and (*b*) lattice parameter b against the mean B–O bond length for hollandites refined in this work and earlier literature.

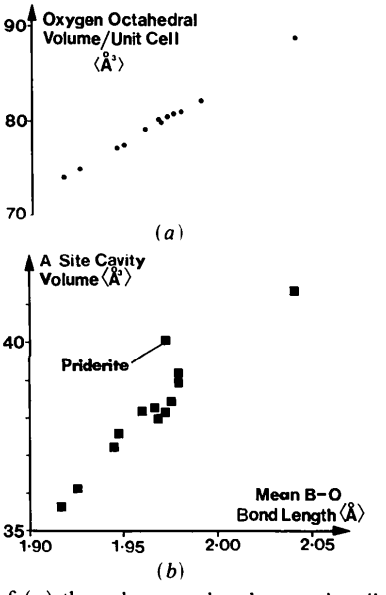

Fig. 3. Plots of (*a*) the volume enclosed per unit cell by the O octahedra V_O and (*b*) the volume enclosed within each A-site cavity V_A against the mean B–O bond length for the hollandites refined in this work and earlier literature.

the O octahedra. Refined data from X-ray single-crystal studies (*i.e.* Dryden & Wadsley, 1958; Cadée & Verschoor, 1978; Sinclair *et al.*, 1980; Schmactel & Muller-Buschbaum, 1980; Post *et al.*, 1982) are also included on these figures and Fig. 6 to present a better overall view of the behaviour of hollandites.

Although the detailed shapes of the O octahedra may change when different *A* and *B* ions occupy the structure, the total octahedral volume V_O displays a remarkably linear dependence on the average *B*–O bond length. The large-scale dimensional characteristics of the tunnel walls, therefore, are controlled by the *B* ions and not by the *A* ions in the tunnels. The distortions in the individual O octahedra can be explained by considering the (010) projection of an octahedral wall shown in Fig. 4. The *B* cations in each column are shifted off-centre in opposite directions because of the mutual repulsion between adjacent columns of *B* ions. All the shifts are parallel to the (010) plane and primarily along the projected line joining adjacent *B* sites (*i.e.* along the triad axis of each octahedra). The outcome of this off-centring is three long *B*–O bonds to the common-edge oxygens and a shortened O–O separation at the common edge caused by the attractive force of the *B* cations (Megaw, 1973). As a consequence the *B* ions make contact with the corner-shared oxygens and increase the O–O separation (refer to Fig. 4).

The lattice parameter *b*, cell volume V_c and *A*-site cavity volume V_A (*i.e.* the volume enclosed by the eight nearest-neighbour O ions surrounding each *A* ion) also display an almost linear dependence on the *B*–O bond length reaffirming the earlier observations of Post *et al.* (1982) that large unit cells are obtained with large *B* cations. This arises because an increase in the *B*–O bond length will also increase the edge length of the O octahedra in the **b** direction as well as the lateral dimensions of the octahedral walls [*i.e.* the O3(2)–O1(4) and O1(4)–O2(1) separations shown in Fig. 1]. Even so, the scatter of the data, particularly V_A, indicates that the influence of the *A*-site cations cannot be completely ignored. When an *A* cation does not completely fill the O cavity, as in barium hollandites, it will occupy an off-centre position and the unit-cell volume and cavity volume V_A will be determined by the size of the *B* ions. When a large ion occupies an *A* site it can, if large enough, expand the *A*-site cavity and thereby enhance the unit-cell volume. This occurs in priderite (Post *et al.*, 1982) where the 'natural' tunnel cavity volume is not quite large enough for K ions. When these ions occupy the *A* sites the octahedral walls are compressed slightly [*i.e.* O1(1)–O1(4) separation decreases] and extended along a perpendicular direction [*i.e.* O3(2)–O2(1) separation increases]. The results for priderite are highlighted in Figs. 2(*a*) and 3(*b*).

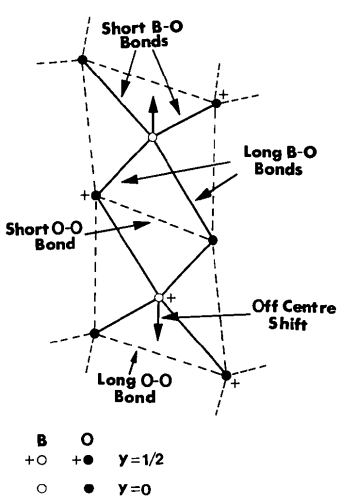

Fig. 4. A (010) projection of the O octahedra in a tunnel wall showing the off-centre shifts of the *B* ions and the relative O–O and *B*–O bond lengths.

In barium hollandites the off-centre Ba ions possess four contact bonds and four non-contact bonds with the surrounding oxygens. The off-centre shift will therefore be determined primarily by the size of the Ba ion for a particular cavity size. The local ordering of the Ba ions observed in nearly all hollandites (Bursill & Grzinic, 1980; Pring, 1983; Kesson & White, 1986), however, will also contribute to the off-centring because of the electrostatic repulsion between ions on adjacent *A* sites. When a particular ordered configuration has a high stabilization energy the contact bond length will be reduced. In the SYNROC-related hollandites for which data are available the contact bond length ranges from 2·734 (4) Å in $Ba_{1\cdot23}(AlTi)_8O_{16}$ to 2·801 Å in $Ba(Ti^{3+}Ti^{4+})_8O_{16}$. It is also worth remarking that the large temperature factors of the Ba ions observed ($B = 2$ Å^2 or greater) in this and earlier work (*e.g.* Sabine & Hewat, 1982) probably reflect some degree of positional disorder of the ions arising from variations in the electrostatic repulsion from site to site.

The tetragonal–monoclinic transformation

As a rule hollandites with large *A* ions and small *B* ions are tetragonal whereas those with small *A* ions and large *B* ions are monoclinic. The distortion in monoclinic hollandites occurs because the tunnel ions are unable to support the octahedral walls which collapse onto the tunnel ions. In this collapse, which is illustrated in Fig. 5, the octahedral walls behave more or less as a rigid framework with the corner linkages acting as a hinge in the [010] direction. In tetragonal hollandites the hinge angles φ and ψ (defined in Fig. 1) are the same and typically between 97 and 98°. In the monoclinic hollandite $Ba_x(FeTi)_8O_{16}$, $x = 1\cdot28$, φ is 104·3° and ψ is 92°. It is possible to convert a monoclinic into a tetragonal hollandite by substituting larger ions into the *A* site. This happens, for instance, when Cs is substituted

into $Ba_x(FeTi)_8O_{16}$, $x = 1{\cdot}28$, which reverts to tetragonal at the composition $Ba\,Cs_{0{\cdot}12}(FeTi)_8O_{16}$.

The boundary between monoclinic and tetragonal hollandites proposed by Post *et al.* (1982), $R_A/R_B = 2{\cdot}08$, does not apply to all hollandites and it is not possible to determine with any certainty the symmetry a particular combination of ions will adopt solely on the basis of their ionic radii. The structural conditions separating the two groups of hollandites, however, do appear to be well defined (see Fig. 6). In this figure R_{AO} is the average distance between the centre of the *A* site (0, 0, 0) and its eight coordinating O ions, and R_{AB} is the average distance between the centre of the *A* site and the four nearest-neighbour *B*-site ions [*i.e.* *B*1(1), *B*1(2), *B*1(3) and *B*1(4)]. The dashed line drawn in Fig. 6 was fitted manually and represents the boundary between the two groups of hollandites (*viz.* $R_{AB} = 1{\cdot}13R_{AO} + 0{\cdot}345$). These results imply that the change in the symmetry depends on a next-nearest-neighbour interaction between the *A* and *B* ions as is often the case in mixed metal oxides (O'Keeffe, 1977). If the size of the *A*-site cavity in a monoclinic hollandite is increased with little or no change in the mean *A*–*B* separation the symmetry can be raised to tetragonal. Alternatively, when the *A*–*B* separation is increased in a tetragonal hollandite without changing the size of the *A*-site cavity, the symmetry will eventually be lowered to monoclinic.

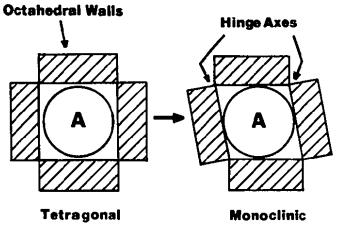

Fig. 5. A simplified picture of the tetragonal–monoclinic transformation in hollandites showing the collapse of the octahedral walls.

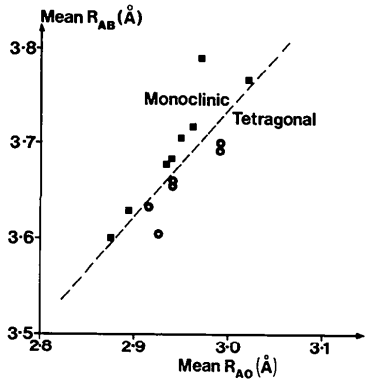

Fig. 6. Plot of the average separation between the centre of the *A*-site cavity and its four nearest-neighbour *B* ions (R_{AB}) against the average distance between the centre of the *A* site and the eight surrounding oxygens (R_{AO}). The dotted line indicates the estimated monoclinic and tetragonal boundary.

Although these changes can be induced by varying the average ionic radii other factors, such as the electrostatic interaction between the *A* and *B* ions and ordering of the *A* and *B* ions on their sites, also contribute to the stability of hollandites.

The progressive changes in structure that occur across a tetragonal–monoclinic boundary are shown in Figs. 7, 8 and 9 for the solid-solution series $Ba([FeAl]_QTi)_8O_{16}$. In Fig. 7 the lattice parameters *a*, *b*, *c*, β and the cell volume V_c clearly identify the transition at $Q = 0{\cdot}57$ (1) and at unit-cell composition estimated to be $Ba_{1{\cdot}23}(Al_{1{\cdot}05}Fe_{1{\cdot}42}Ti_{5{\cdot}53})O_{16}$. Above and below this boundary the lattice parameters display a substantially linear dependence on *Q* and are continuous across the boundary. The unit-cell volume, however, undergoes a discontinuous decrease in the slope dV_c/dQ at the boundary. As the lattice parameter *b* and its derivative db/dQ appear to be continuous across the boundary, the decrease in dV_c/dQ reflects a change in the packing efficiency within the (010) planes of the structure. The manner in which the tunnel collapse occurs is indicated in Fig. 8 which shows the hinge angles φ and ψ plotted against *Q* along with the deformation angles γ and δ of the octahedral walls (all these angles are defined in Fig. 1). Across the monoclinic domain the hinge angle φ increases from ~98° at the phase boundary to ~104° at $Q = 1$ whilst the complementary angle ψ decreases from ~96° down to ~92°. On approaching the phase boundary from the monoclinic side the two hinge angles do not converge to the same value at the phase boundary. In crossing the phase boundary the structure transforms discontinuously with the difference $\varphi - \psi$ changing from

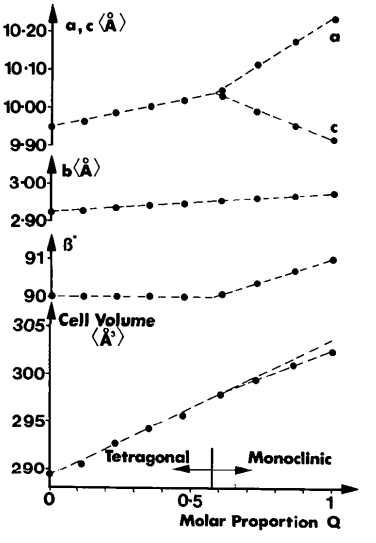

Fig. 7. Variation of the lattice parameters *a*, *b*, *c* and β along with the unit-cell volume for the solid-solution series between $Ba_{1{\cdot}23}(AlTi)_8O_{16}$ and $Ba_{1{\cdot}28}(FeTi)_8O_{16}$ where *Q* is the molar proportion of $Ba_{1{\cdot}28}(FeTi)_8O_{16}$.

~2° on the monoclinic side to zero as soon as it becomes tetragonal.

The increase in φ across the monoclinic domain is ~6° whereas the decrease in ψ is only ~4°. For a model of tunnel-wall collapse involving hinging about the corner linkages and a rigid wall structure, the changes in φ and ψ would be equal and opposite. The departure from this condition indicates that the tunnel walls do not behave as a perfectly rigid framework. A small distortion develops as Q increases which is manifested by a decrease of ~1° in each of the deformation angles γ and δ. Over the monoclinic range the O1(1)–O1(4) and O4(1)–O4(4) common edge lengths do not change. The only O–O separations in the (010) projection that show any substantial change over this region are those between the corner linkages [*e.g.* O3(2)–O2(4)]. This contrasts with the tetragonal domain where the growth of the O octahedra is the result of elongation of all the edges.

Unlike the tetragonal phase, the *S*- and *T*-type octahedra are no longer equivalent. The plot of volume per O octahedron for each of these types between $Q = 0$ and 1 is shown along with the *A*-site cavity volume in Fig. 9. The fact that the *S*-type octahedra enclose a larger volume raises the possibility of partitioning of the ions between the two types of octahedra. The data only give limited support to this suggestion. In $Ba_{1\cdot28}(FeTi)_8O_{16}$ the average *B*–O bond length is 1·983 (5) Å in *S*-type octahedra and 1·979 (5) Å in *T*-type octahedra. Also, when the occupancies of the Fe and Ti ions on these octahedra are refined separately there is no significant difference in the observed occupancy levels [*i.e.* 1·29 (2) Fe ions/cell in *S* type and 1·27 (2) Fe ions/cell in *T* type]. The difference in the volumes of these octahedra can probably be attributed to the *T*-type octahedra being in closer contact with the *A* ions than the *S*-type octahedra. This is supported by the fact that the wall deformation angle δ associated with the *T*-type octahedra is less than the corresponding angle γ associated with the wall of *S*-type octahedra. Over this region both the occupancy of the *A* sites and the rate of growth of the *A*-site cavity volume (see Fig. 9*b*) increase and both the *S*- and *T*-type octahedra have smaller volumes than would be expected if the rate of increase over the tetragonal domain were to continue into the monoclinic domain.

Conclusions

Of the hollandites refined in this work $Ba_{1\cdot28}(FeTi)_8O_{16}$ appears to have the optimum structural properties for the substitution of large ions on the *A* sites. First, it has the largest *A*-site cavity volume. Second, the tunnel framework has collapsed more than the other hollandites and it is therefore able to accommodate substituted ions up to the transformation boundary without deforming the tunnel walls. Once in the tetragonal state the maximum level of substitution will depend on the amount of deformation the tunnel walls can tolerate. The SYNROC hollandites currently being evaluated for radwaste disposal are similar to the solid solutions considered here except that Ti^{3+} ions occupy the *B* sites rather than Fe^{3+} ions. As these ions are larger than Fe^{3+} ions, hollandites containing Ti^{3+} will possess larger *A*-site cavity volumes and would be expected to accommodate higher concentrations of Cs.

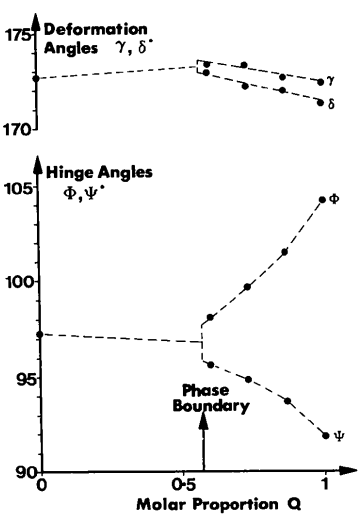

Fig. 8. Variation of the deformation angles γ and δ within the tunnel wall and the hinge angles φ and ψ between the tunnel walls for the solid solutions between $Ba_{1\cdot23}(AlTi)_8O_{16}$ and $Ba_{1\cdot28}(FeTi)_8O_{16}$ where Q is the molar proportion of $Ba_{1\cdot28}(FeTi)_8O_{16}$.

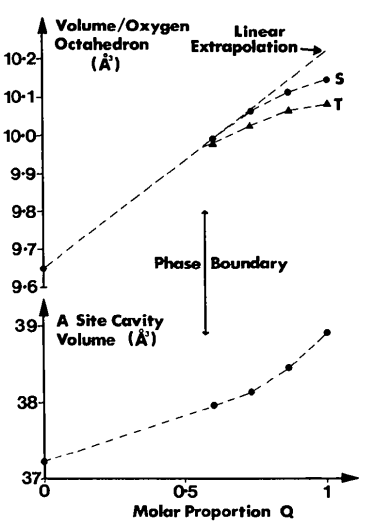

Fig. 9. Plots of the volumes enclosed by the *S*- and *T*-type octahedra for the solid solutions between $Ba_{1\cdot23}(AlTi)_8O_{16}$ and $Ba_{1\cdot28}(FeTi)_8O_{16}$ where Q is the molar proportion of $Ba_{1\cdot28}(FeTi)_8O_{16}$.

I wish to acknowledge the support given to this work by the Australian Atomic Energy Commission (Research Contract No. 82/X/1) and the Australian Institute of Nuclear Science and Engineering. I am also grateful to Joanne Hodge and Suzanne Swanson for their assistance during the course of this investigation.

References

BURSILL, L. A. & GRZINIC, G. (1980). *Acta Cryst.* B**36**, 2902-2913.
BYSTRÖM, A. & BYSTRÖM, A. M. (1950). *Acta Cryst.* **3**, 146-154.
CADÉE, M. C. & VERSCHOOR, G. C. (1978). *Acta Cryst.* B**34**, 3554-3558.
CHEARY, R. W., HUNT, J. V. & CALAIZIS, P. (1981). *J. Aust. Ceram. Soc.* **17**, 11-12.
CHEARY, R. W. & KWIATKOWSKA, J. C. (1984). *J. Nucl. Mater.* **125**, 236-243.
DRYDEN, J. C. & WADSLEY, A. D. (1958). *Trans. Faraday Soc.* **54**, 1574-1580.
GUHA, J. P., KOLAR, D. & VOLAVSEK, B. (1976). *J. Solid State Chem.* **16**, 49-54.
HOWARD, C. J. (1982). *J. Appl. Cryst.* **15**, 615-620.
HOWARD, C. J., BALL, C. J., DAVIS, L. D. & ELCOMBE, M. M. (1983). *Aust. J. Phys.* **35**, 507-518.
KESSON, S. E. (1983). *Rad. Waste Manage.* **4**, 53-72.
KESSON, S. E. & RINGWOOD, A. E. (1984). *Scientific Basis for Nuclear Waste Management.* VI, pp. 507-512. Amsterdam: Elsevier.
KESSON, S. E. & WHITE, T. J. (1986). *Proc. R. Soc. London Ser. A.* In the press.
KLUG, H. P. & ALEXANDER, L. E. (1974). *X-ray Diffraction Procedures*, ch. 8, pp. 566-617. New York: Wiley-Interscience.
MEGAW, H. D. (1973). *Crystal Structures: A Working Approach*, pp. 333-334. London: Saunders.
O'KEEFFE, M. (1977). *Acta Cryst.* A**33**, 924-927.
POST, J. E., VON DREELE, R. B. & BUSECK, P. R. (1982). *Acta Cryst.* B**38**, 1056-1065.
PRING, A. (1983). PhD thesis, Univ. of Cambridge.
RIETVELD, H. M. (1969). *J. Appl. Cryst.* **2**, 65-71.
ROTH, R. (1981). Annual Report. National Measurement Laboratory, Office for Nuclear Technology. NBSIR 81-2241.
SABINE, T. M. & HEWAT, A. W. (1982). *J. Nucl. Mater.* **110**, 173-177.
SCHMACTEL, J. & MULLER-BUSCHBAUM, H. K. (1980). *Z. Naturforsch. Teil B*, **35**, 332-334.
SINCLAIR, W., MCLAUGHLIN, G. M. & RINGWOOD, A. E. (1980). *Acta Cryst.* B**38**, 245-246.
WILES, D. B. & YOUNG, R. A. (1981). *J. Appl. Cryst.* **14**, 149-150.

Acta Cryst. (1986). B**42**, 236-247

Determination of the Structure of Cu_2ZnGeS_4 Polymorphs by Lattice Imaging and Convergent-Beam Electron Diffraction

BY A. F. MOODIE AND H. J. WHITFIELD

Division of Chemical Physics, CSIRO, PO Box 160, *Clayton, Victoria, Australia* 3168

(*Received* 2 *May* 1985; *accepted* 22 *November* 1985)

Abstract

The structures of two polymorphs of Cu_2ZnGeS_4 have been determined by the use of convergent-beam electron diffraction (CBED) and high-resolution lattice imaging with 200 kV electrons. A tetragonal polymorph with space group $I\bar{4}2m$ and axes $a = 5{\cdot}27$, $c = 10{\cdot}54$ Å was found to be isostructural with Cu_2FeSnS_4. The second polymorph has a pseudo-rhombohedral structure related to $12R$ ($|+++-|_3$) ZnS by ordered replacement of three-quarters of the Zn atoms by Cu and Ge. It can be described in terms of a triply primitive cell with orthogonal axes $a = 36{\cdot}6$, $b = 6{\cdot}55$ and $c = 7{\cdot}52$ Å. The S-atom positions of a trial ideal structure were refined by use of CBED and lattice images. Stacking faults and edge and screw dislocations were observed in this structure in high-resolution lattice images.

Introduction

We have shown previously (Moodie & Whitfield, 1983) that the stacking sequence in small volumes of normal tetrahedral structures can be determined, using a 200 kV electron microscope, and we have illustrated the technique with the compound CuAsSe.

For ternary and quaternary chalcogenides such as 1_246_3 and 1_2246_4 the degree of ordering of metal ions depends on the thermal history of the sample. Furthermore small deviations in stoichiometry can determine the final structure (*e.g.* Cu_2GeS_3) while different polytypes may be stable at high and low temperatures (*e.g.* $CuSiS_3$).

We have found that convergent-beam electron diffraction combined with high-resolution lattice imaging allows both characterization and structure determination on crystal fragments from a matrix

0108-7681/86/030236-12$01.50